Microchimica Acta
https://doi.org/10.1007/s00604-017-2629-x

ORIGINAL PAPER

Immobilization of horseradish peroxidase on amino-functionalized carbon dots for the sensitive detection of hydrogen peroxide

Ya Su[1] · Xuan Zhou[1] · Yumei Long[1,2,3] · Weifeng Li[1]

Received: 8 September 2017 / Accepted: 22 December 2017

Abstract

The authors describe the preparation of amino-functionalized carbon dots (NH_2-CDs) via a one-step hydrothermal process using silver nitrate and chitosan as the precursors. The NH_2-CDs have a fairly consistent size distribution with an average size of 2.8 ± 0.5 nm. This is attributed to the introduction of Ag(I) both as a catalyst and a precipitant. The NH_2-CDs are highly crystalline. Their surface carries amino groups and carboxy groups which is confirmed by transmission electron microscopy (TEM) and Fourier transform infrared (FTIR) spectroscopy. Horseradish peroxidase (HRP) was immobilized in the NH_2-CDs and then placed on a glassy carbon electrode (GCE). Spectroscopic and electrochemical analyses evidenced the stability and good bioactivity of the immobilized HRP. This reveals that NH_2-CD is a desirable matrix for enzyme immobilization. The modified GCE exhibits enhanced electro-catalytic activity towards hydrogen peroxide (H_2O_2) reduction as compared to that of plain CDs. The effects of pH value and loading on the performances of the modified GCEs were studied. Under optimized conditions, the biosensor has a linear response in the 5 to 590 nM H_2O_2 concentration range, with a 1.8 nM defection limit (at an S/N ratio of 3). The sensor is stable, reproducible and selective. Finally, the sensor was applied to determine H_2O_2 in real samples, and satisfactory recoveries were achieved.

Keywords Hydrothermal method · Electro-catalytic reduction · Glassy carbon electrode · Cyclic voltammetry · Amperometric response · Biosensor · H_2O_2 · Analytical property

Introduction

Hydrogen peroxide (H_2O_2) is an important intermediate in environmental, biochemical and medicinal reactions. It is also commonly used in industrial processes as oxidant [1–3]. However, high H_2O_2 concentrations would be harmful to human beings [4]. Thus, accurate and rapid determination of H_2O_2 is of great significance. Various techniques have been developed for the determination of H_2O_2. Among them, electrochemical sensors have been proved to be a promising method due to their rapid response, low cost and easy operation. Particularly, based on the intrinsic sensitivity and selectivity of enzymatic reactions, enzyme-based electrochemical sensors have become one of the most powerful tools in many areas, such as food analysis, environmental monitoring and clinical diagnosis [2, 5, 6].

HRP is commercially available heme enzyme with high-purity and has been widely used to fabricate biosensors for the detection of H_2O_2 or related compounds [7–9]. These biosensors are based on the direct electron transfer between enzymes and the underlying electrodes. However, the direct electron transfer between enzymes and the underlying electrodes is often difficult to achieve because of the deeply buried redox-active center, unfavorable orientation and adsorptive denaturation [10–12]. To overcome these drawbacks, nanomaterials have been

Electronic supplementary material The online version of this article (https://doi.org/10.1007/s00604-017-2629-x) contains supplementary material, which is available to authorized users.

✉ Yumei Long
yumeilong@suda.edu.cn

✉ Weifeng Li
liweifeng@suda.edu.cn

[1] College of Chemistry, Chemical engineering and Materials Science, Soochow University, Suzhou, Jiangsu 215123, People's Republic of China

[2] The Key Lab of Health Chemistry and Molecular Diagnosis of Suzhou, Suzhou, People's Republic of China

[3] State Key Laboratory of Chemo/Biosensing and Chemometrics, Hunan University, Changsha 410082, People's Republic of China

Published online: 15 January 2018

popularly employed as immobilization matrix in the fabrication of enzyme-based biosensors [13–16].

Carbon dots are a new emerging type of carbon-based nanomaterials with a size of less than 10 nm [12]. They have aroused increasing research interests owing to their promising properties, such as robust chemical inertness, fascinating optical properties, good electrochemical activity, and excellent bio-compatibility [17–20]. CDs are generally discrete and quasi-spherical nanoparticles comprising amorphous or nanocrystalline cores [21]. Their properties can be improved by tuning the chemical structure, which are strongly dependant on the preparation methods and precursors used for synthesis [22].

In addition to excellent luminescence properties [23, 24], CDs also demonstrated promising electrocatalytic activity [25–27]. Both theoretical calculation and experiments showed that CDs possess high electron density and electron mobility, which make them interesting contenders as electrocatalytic and electrochemical materials [18]. Meanwhile, the surface of CDs can be easily modified by functional groups through changing precursors. These functional groups, such as amino and carboxylic groups will endue CDs suitable for further functionalization with various inorganic, organic, polymeric, or biological species [28–30]. Thus, it is interesting to study the interaction between CDs and enzymes, and further to explore their application for biosensor fabrication.

In this paper, NH2-CDs were synthesized through hydrothermal method using chitosan as a precursor. The structure and surface properties of NH2-CDs were investigated. Then, NH2-CDs were employed as matrix for HRP immobilization to construct a novel H2O2 biosensor. The biosensor exhibited excellent analytical properties and this approach was successfully applied for real sample assay.

Experimental section

Materials and reagents

HRP (EC 1.11.1.7, Type II, 300 $U \cdot mg^{-1}$), quercetin hydrate (QC), uric acid (UA), ascorbic acid (AA) and dopamine (DA) were purchased from Sangon Biotech Co. Ltd., Shanghai, China (http://www.sangon.com/). Tea polyphenol (TP) was purchased from Adamas Reagent, Ltd. (http://www.adamas-beta.com/). Other reagents obtained from Sinopharm Chemical Reagent Co. Ltd. (http://www.sinoreagent.com/) are analytical grade and used without further purification. The phosphate buffer was chosen as the supporting electrolyte. Their pH values were adjusted by mixing 0.2 M Na_2HPO_4 and 0.2 M NaH_2PO_4 in different volumes. Double distilled water was used throughout the experiments.

Preparation of amino-functionalized CDs

NH_2-CDs were synthesized by a hydrothermal method using chitosan as carbon source. Typically, 0.1 g of chitosan was dissolved in 38 mL of acetic acid solution (1%, containing 1 mM $AgNO_3$) under vigorously stirring. Subsequently, the mixture was transferred into a Teflon-equipped stainless steel autoclave (50 mL in volume) and the filling rate is 80%. Then, the autoclave was kept in the furnace at 160 °C for 3 h. When the autoclave cooled down to room temperature, the suspension was centrifuged at 12000 rmp for 15 min and the precipitates were discarded. The upper dark yellow solution was NH_2-CD aqueous solution. Finally, the suspension was dried until the powder was obtained. For comparison, carbon dots were obtained by the same way, except that glucose was used as precursor instead of chitosan.

Preparation of the HRP/NH_2-CD modified glassy carbon electrode

Prior to use, a GCE (0.5 cm in diameter) was firstly polished with 1.0, 0.3, and 0.05 μm alumina slurries (Aida Hengsheng Co. Ltd., Tianjin, China http://www.tjaida.cn/) repeatedly to obtain a mirror-like surface, followed by successive sonication in ethanol and double distilled water for 10 min, respectively. Secondly, the electrode was pretreated electrochemically, in H_2SO_4 aqueous solution (1.0 M) and in double distilled water successively. The cycling potential was from −1.0 to 1.0 V at a scan rate of 100 $mV \cdot s^{-1}$ until a stable cyclic voltammogram was obtained. Then the electrode dried in a flow of nitrogen. Thirdly, the mixture containing 10 μL of NH_2-CD solution (0.5 $mg \cdot mL^{-1}$) and 10 μL of HRP solution (1 $mg \cdot mL^{-1}$) was spread onto the surface of GCE and dried at 4 °C to form a film. Finally, 2 μL of Nafion (1% dissolved in anhydrous ethanol, Sigma-Aldrich, www.sigmaaldrich.com/china-mainland.html) was used as a binder to hold the NH_2-CD-HRP film tightly on the surface of the GCE. This modified electrode is denoted as GCE/NH_2-CD-HRP/Nafion. In the control experiments, GCE/NH_2-CD/Nafion, GCE/HRP/Nafion and GCE/CD-HRP/Nafion were also fabricated by a same way. Before electrochemical examinations, all the modified electrodes were washed by phosphate buffer (pH = 7.0) to remove residual components.

Instruments and measurements

The morphologies and microstructures of the samples were observed by TEM (Tecnai G220, FEI, America, an acceleration voltage of 200 kV). FTIR spectroscopy (Nicolet 380, Thermo Nicolet, America) was employed to characterize functional groups using KBr (Sinopharm Chemical Reagent Co. Ltd. http://www.sinoreagent.com/) pellet preparation technique. UV-Vis absorbance spectra were obtained on TU-

1810 UV-Vis spectrophotometer (Beijing Purkinje General Instrument Co. LTD., China, www.pgeneral.com). The NH2-CD-HRP solution was prepared by mixing HRP and NH2-CD in phosphate buffer under stirring and further incubating for 12 h. Then, the solution was casted on a quartz glass slide and dried at room temperature. In the same way, quartz glass slides with HRP and NH2-CD films, respectively, were also prepared for UV-Vis measurements. Chemical states of elements were analyzed by X-ray photoelectron spectroscopy (XPS), recorded on an Axis Ultra HAS X-ray photoelectron spectrometer using Al Kα radiation (1486.6 eV).

Cyclic voltammetry (CV) measurements were performed with a CHI611D electrochemical workstation (Chenhua Instruments Co., China, www.chinstruments.com). The CV measurements were based on a conventional three-electrode system, which includes a platinum electrode (counter electrode), a Ag|AgCl electrode (saturated KCl) (eference electrode), and a modified electrode (working electrode), respectively. CVs were recorded in the range from −1.0 to 1.0 V. Electrochemical impedance spectroscopy (EIS) was performed on a RST5200 electrochemical workstation (Suzhou Risetest Instrument Co. LTD., China, www.rst0000.com) in the presence of 0.1 M KCl containing 0.1 mM $[Fe(CN)_6]^{3-/4-}$ (1:1) mixture. All the electrochemical measurements were performed in phosphate buffer at room temperature (25 ± 2 °C).

Results and discussion

Characterization of the samples

In order to obtain uniform CD particles, Ag^+ ions were introduced to act as catalyst and precipitant. Under hydrothermal condition, Ag^+ ions are easily reduced by aldehyde groups of chitosan (or glucose) to produce Ag nanoparticles. The good catalytic activity of Ag nanoparticles will promote carbonization of chitosan (or glucose) to form CDs. Meanwhile, Ag nanoparticles combine with carbon to form heterostructures with large size and they are easily removed by centrifugation [31].

Figure 1a shows TEM images of NH_2-CDs (chitosan) sample. NH_2-CDs are spherical and uniform dispersion. The average particle diameter is estimated to be 2.8 ± 0.5 nm based on statistical analyses of 100 dots (inset of Fig. 1a). The similar microstructure can also be observed for CDs (glucose) sample (Fig. S1A and S1B in supporting information). The high-resolution TEM (Fig. 1b) illustrates well-resolved lattice fringes with an interplanar spacing of 0.208 nm, which is close to the (100) facet of graphitic carbon [25]. The results suggest that the NH_2-CDs consist of crystalline graphitic core and a thin amorphous shell.

Figure 2 shows FTIR spectra of samples. NH_2-CDs exhibit a broad absorption band extending from 3000 cm^{-1} to 3700 cm^{-1}, which correspond to ν(O-H) and ν(N-H) stretching vibrations. Absorption bands centered at 1726 cm^{-1} and 1635 cm^{-1} are assigned to the C=O vibration in COOH and CONH, respectively. Absorption bands peaking at 1405 cm^{-1} and 1224 cm^{-1} originate from the bending vibrations of C-H and the stretching vibrations of C-N, respectively. The results evidence the successful amino-functionalization of CDs. These amino radicals should inherit from chitosan during carbonization. These functional groups can improve the adsorbing ability of NH_2-CDs to biomolecules and make them potential applications for biosensing.

The chemical compositions of samples were analyzed by XPS technique, as shown in Fig. S2 (in Supporting Information). Both C and O occur in CDs and NH_2-CDs

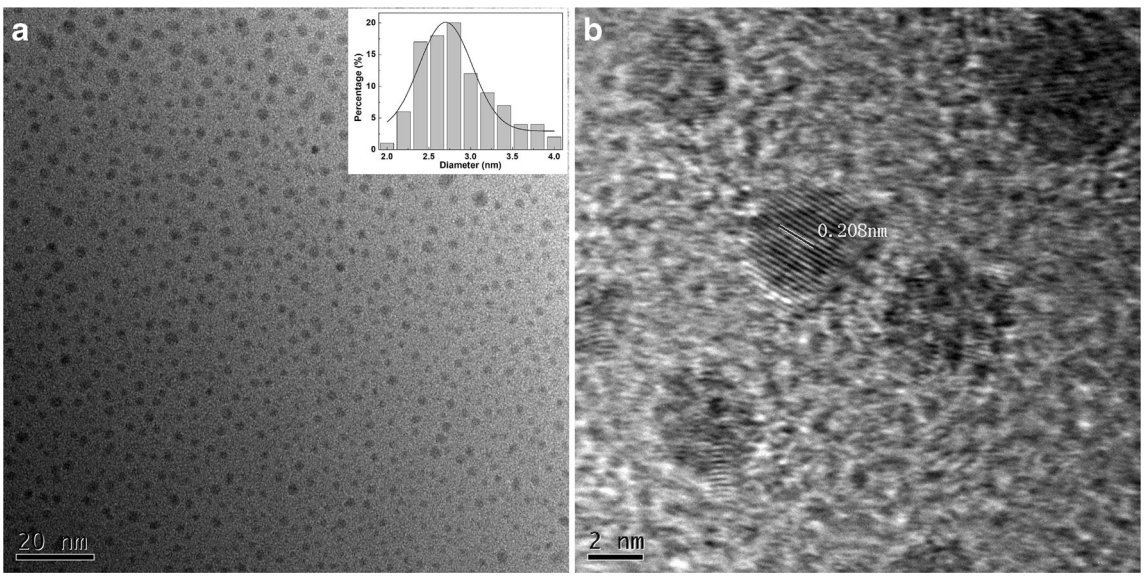

Fig. 1 TEM (**a**) and high-resolution TEM (**b**) images of amino-functionalized carbon dots (NH_2-CDs). Inset is the size distribution of NH_2-CDs

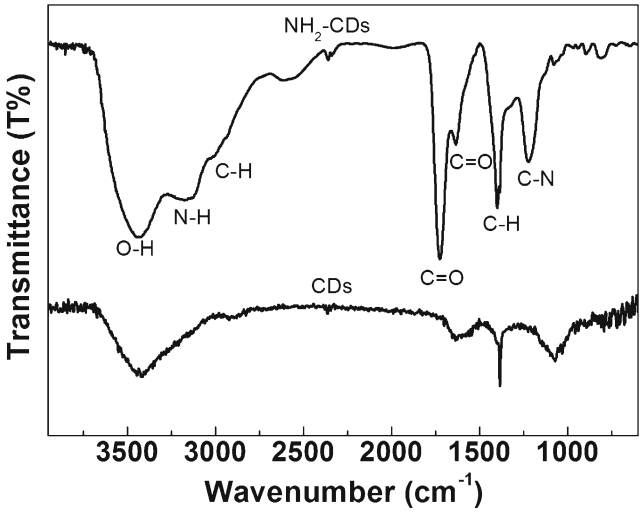

Fig. 2 FTIR spectra of CDs and NH_2-CDs

samples. However, N only exists in the NH_2-CDs sample, which agrees well with FTIR results (Fig. 2). Moreover, no XPS signal can be discernible corresponding to silver, indicating that the Ag nanoparticles have been completely removed from the system.

Fig. S3A (in Supporting Information) displays the optical absorption spectra of NH_2-CDs, HRP and NH_2-CD-HRP, respectively. An absorption band at 280 nm for CDs sample can be observed, consistent with previous reports [32]. The spectrum of HRP shows a broad absorption band centered at 403 nm, which is the characterized Soret absorption. The Soret band of protein is sensitive to the variation of the micro-environment around the heme group [33]. Fig. S3A shows that the Soret band of NH_2-CD-HRP is quite similar to that of HRP. It means that the combination with NH_2-CDs has not degraded the structure of HRP. Further Supporting Information can be achieved from FTIR spectra (Fig. S3B in Supporting Information). NH_2-CD-HRP nearly shows the same FTIR spectrum to that of HRP in the absorption band of amide I (1647 cm^{-1}) and amide II (1540 cm^{-1}) [34], respectively. These results also reveal that the HRP immobilized by NH_2-CDs has the same structure to that of native HRP.

The interface properties of the electrodes modified by different substances were studied using EIS technique. Fig. S4 (in Supporting Information) shows the Nyquist plots of the modified electrodes in a solution of 0.1 M KCl containing 0.001 M $K_4Fe(CN)_6/K_3Fe(CN)_6$. All the EIS curves are composed of a semicircle portion at higher frequencies representing the charge-transfer resistance (R_{ct}), and a linear section at lower frequencies standing for the diffusion limited process [35]. The modified electrodes exhibit increased R_{ct} values as compared to that of the bare GCE (curve a). The R_{ct} values of GCE/CD/Nafion (curve b) and GCE/NH_2-CD/Nafion (curve c) are slightly increased, respectively, indicating that the functionalized surface obstruct the electron transfer. On the other hand, GCE/HRP/Nafion (curve f) has the largest R_{ct} value, which is attributed to an insulating protein layer of HRP, hindering the electron transfer of the redox probe to the electrode surface. The introduction of NH_2-CDs (or CDs) into the GCE/HRP/Nafion causes a significant decrease of R_{ct} (curves d and e). This indicates that NH_2-CDs (or CDs) enhance the electron transfer. Especially, GCE/NH_2-CD-HRP/Nafion exhibits a smaller R_{ct} value (curve e) than that of GCE/CD-HRP/Nafion (curve d), suggesting that NH_2-CDs are better than CDs in the immobilization of HRP.

Electrochemical properties of biosensors

Figure 3 shows cyclic voltammetry (CVs) on different electrodes in 0.2 M phosphate buffer (pH 7.0) at a scan rate of 0.1 $V{\cdot}s^{-1}$. No redox peaks can be identified at the GCE/Nafion (Fig. 3a), GCE/CD/Nafion (Fig. 3b) and GCE/NH_2-CD/Nafion (Fig. 3c), indicating that Nafion, CD/Nafion and NH_2-CD/Nafion are electro-inactive in the investigated potential window. On the other hand, all the HRP-electrodes present an obvious cathodic peak at −0.286 V (vs. Ag/AgCl). This cathodic peak is ascribed to the reduction of HRP at the underlying electrodes. Moreover, the peak currents increase with the introduction of CDs (Fig. 3b) and NH_2-CDs (Fig. 3c), and the best current response is achieved at GCE/NH_2-CD/Nafion. It is 4.7 times and 2.03 times as large as those of GCE/HRP/Nifion and GCE/CD-HRP/Nafion, respectively. The excellent electrochemical property of GCE/NH_2-CD/Nafion is attributed to the unique microstructure of NH_2-CDs. First, the quantum size effect of CDs can improve HRP immobilization in the film. Second, amino- and carboxyl- groups at the surface of NH_2-CDs provide a number of sites for HRP attachment. Furthermore, the crystalline graphitic cores of NH_2-CDs have good conductivity and they can act as microelectrodes to connect the active sites of HRP with the underlying electrode. As a result, the distance between the active site of HRP and the microelectrodes was smaller than the original distance between the enzyme and the electrode surface. Because the rate coefficient of electron transfer between the donator and acceptor decrease exponentially with the distance between electron transferring centers, the enzyme activity is increased [36].

Figure 3d presents the CVs of GCE/NH_2-CD-HRP/Nafion in the presence of H_2O_2 with different concentrations. As can be seen, the reduction peak increases with the increase of H_2O_2 concentration. The results illustrate that the immobilized HRP possessed excellent electrocatalytic activity towards H_2O_2 reduction. The electrocatalytic reduction mechanism can be described as follows [37]:

$$\mathrm{HRP}\left(\mathrm{Fe}^{3+}\right) + \mathrm{H_2O_2} \rightarrow \text{Compound I } \left(\mathrm{Fe}^{4+}=\mathrm{O}\right) + \mathrm{H_2O} \quad (1)$$

$$\text{Compound I } \left(\mathrm{Fe}^{4+}=\mathrm{O}\right) + \mathrm{e}^- + \mathrm{H}^+ \rightarrow \text{Compound II} \quad (2)$$

$$\text{Compound II} + \mathrm{e}^- + \mathrm{H}^+ \rightarrow \mathrm{HRP}\left(\mathrm{Fe}^{3+}\right) + \mathrm{H_2O} \quad (3)$$

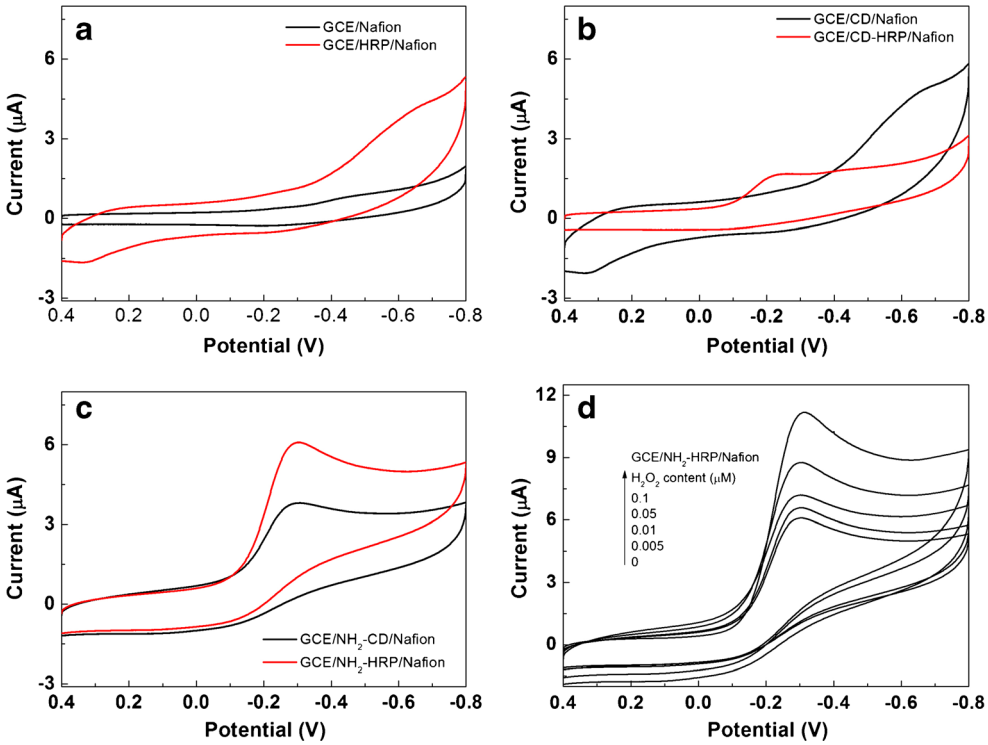

Fig. 3 Cyclic voltammograms (CVs) of GCE/Nafion and GCE/HRP/Nafion (**a**); GCE/CD/Nafion and GCE/CD-HRP/Nafion (**b**); GCE/NH_2-CD/Nafion and GCE/NH_2-CD-HRP/Nafion (**c**); CVs of GCE/NH_2-CD-HRP/Nafion in the presence of different concentrations of H_2O_2 (**d**). Conditions: N_2-saturated phosphate buffer, pH 7.0, scan rate: 0.1 $V{\cdot}s^{-1}$

In which compound I and compound II are intermediates.

Optimization of experimental conditions

In order to achieve desirable biosensor for H_2O_2 detection, some parameters were optimized. Fig. S5A (in Supporting Information) displays amperometric response of the GCE/NH_2-CD-HRP/Nafion at different pH in the presence of 0.1 μM H_2O_2. The current response increases from pH 5.5 and a maximum is obtained at pH 7.0. Further increasing pH (>7.0) leads to the decrease of response current. The results agree well with that for soluble HRP [38], suggesting that the existence of NH_2-CDs did not alter the optimal pH value for catalytic reaction of the immobilized HRP towards H_2O_2. Thus, the 0.2 M phosphate buffer with pH of 7.0 was chosen for later experiments.

Fig. S5B (in Supporting Information) shows current responses of GCE/NH_2-CD-HRP/Nafion towards 0.1 μM H_2O_2 with different concentration ratio between HRP and NH_2-CDs. When the ratio is 2:1, the modified electrode exhibits the best current response. In addition, the deposition volume of solution (HRP/NH_2-CDs = 2) also has effect on the sensitivity of the biosensor. As shown in Fig. S5C (in Supporting Information), the response current (measured in the deoxygenated phosphate buffer 0.2 M, pH 7.0, 0.1 μM H_2O_2, scan rate: 0.1 $V{\cdot}s^{-1}$) increases from volume of 3 μL and reaches a maximum at a volume of 9 μL, then decreases to volume of 15 μL. Moreover, the modified electrode becomes un-stable at higher modifier content. Therefore, the

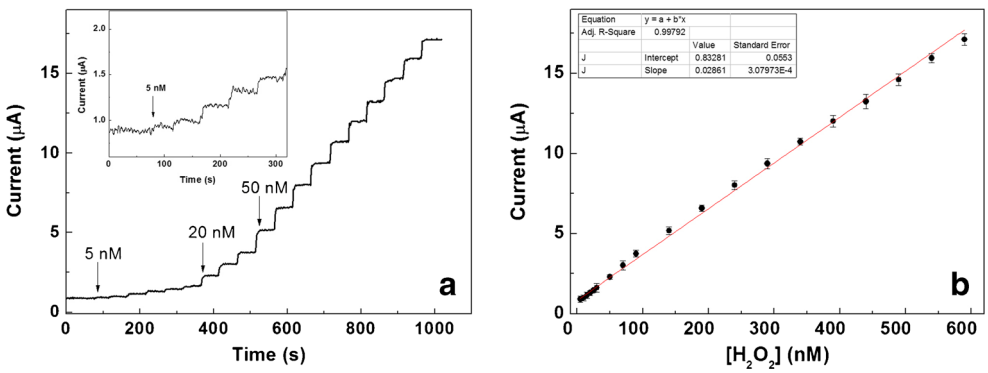

Fig. 4 The chronoamperometric response of GCE/NH_2-CD-HRP/Nafion to H_2O_2 additions in 0.2 M phosphate buffer (pH 7.0) with potential of −0.3 V under stirring. Inset: a magnification of the current response at low H_2O_2 concentrations (**a**); Corresponding calibration curve between currents and H_2O_2 concentrations (**b**)

Table 1 Comparison of various HRP-based biosensors for the detection of H_2O_2

Materials	Linear range (μM)	Detection limit (μM)	Potential (V)	Refs
HRP/C-dots/LDHs	0.1~23.1	0.04	−0.35	[27]
HRP-PGN	0.08 nM~835	0.0267 nM	−0.7	[7]
HRP/TB/CCB	0.429~455	0.17	−0.25	[8]
HRP-MIL100(Cr)-B	0.5~3000	0.1	−0.3	[39]
HRP-BMIM-BF_4/SWCNTs/CFUME	0.49~10.2	0.13	−0.35	[40]
Flower-like Bi_2WO_6	0.5~100	0.18	−0.35	[41]
HRP/Au/PDDA/GO	0.0198~1.04	0.0075	−0.4	[42]
HRP-MoS_2-Gr	0.2~1.103	0.049	−0.08	[43]
Co_3O_4/MWCNTs/gelatin/HRP	0.74~19	0.74	−0.3	[44]
NH-CDs-HRP	0.005~0.59	0.0018	−0.3	This work

BMIM-BF_4: 1-butyl-3-methylimidazolium tetrafluoroborate; SWCNTs: single-walled carbon nanotubes; CFUME: carbon fiber ultramicroelectrode; PGN: porous graphene; MIL100(Cr)-B: boronic acid functionalized metalorganic framewords; PDDA: poly (diallyldimethylammonium chloride); GO: graphene oxide; TB: toluidine blue; CCB: ceramic composite biosensor; Gr: grapheme; MWCNTs: multiwalled carbon nanotubes

concentration ratio of 2:1 (HRP:NH_2-CDs) and deposition volume of 9 μL are adopted.

Amperometric response of H_2O_2

The analytical property of GCE/NH_2-CD-HRP/Nafion was further evaluated by the amperometric method in the detection of H_2O_2. Fig. S5D (in Supporting Information) shows the effect of the applied potential on the steady-state of the GCE/NH_2-CD-HRP/Nafion in the range of −0.1~−0.5 V. The response current strikingly increases with the change of the applied potentials from −0.1 to −0.3 V. As applied potentials are beyond −0.3 V, the response current increases slowly. Hence, the working potential was set at −0.3 V. Figure 4a displays the typical current-time plot at GCE/NH_2-CD-HRP/Nafion with successive injection of H_2O_2 into the stirred phosphate buffer (0.2 M, pH 7.0) under the optimal conditions. The response currents of the sensor exhibit a step-like increase along with H_2O_2 concentrations and a steady state (90% of the maximum value) is achieved within 5 s. The calibration plot (Fig. 4b) illustrates linear relationship between response current and H_2O_2 concentration in the range from 0.005 μM to 0.59 μM, and the detection limit is 0.0018 μM (S/N = 3). The linear regression equation is $I_p = 0.8328 + 0.0286\,[H_2O_2]$ (R = 0.998) and the sensitivity is calculated to be 145 $\mu A \cdot \mu M^{-1} \cdot cm^{-2}$. Table 1 summarized a comparison of analytical performances of the GCE/NH_2-CD-HRP/Nafion with other HRP-based H_2O_2 biosensors. The biosensor in this work exhibits desired analytical properties, which are comparable to and even higher than those of previously reported HRP-based sensors in the determination of H_2O_2. The excellent analytical property is attributed to the rich of functional groups, such as amino radical and hydroxyl on the surface of CDs, which provide friendly environment for HRP.

Figure 5 displays i-t curve of the GCE/NH_2-CD-HRP/Nafion upon the consecutive addition of 0.1 μM H_2O_2 and 0.1 μM interfering substances (in phosphate buffer, pH 7.0, applied potential −0.3 V). As can be seen, the addition of

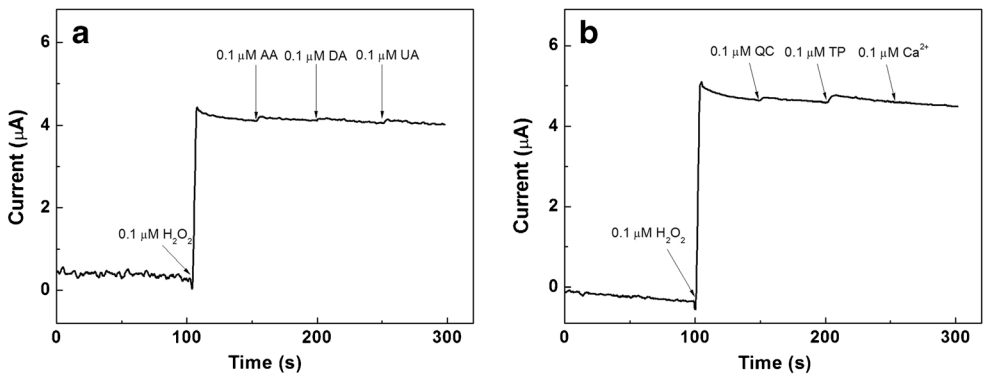

Fig. 5 Amperometric response of GCE/NH_2-CD-HRP/Nafion to 0.1 μM H_2O_2 in the presence of 0.1 μM of ascorbic acid (AA), 0.1 μM of dopamine (DA) and 0.1 μM of uric acid (UA), respectively (**a**), and in the presence of 0.1 μM of quercetin (QC), 0.1 μM of tea polyphenol (TP) and 0.1 μM of calcium, respectively (**b**). Conditions: 0.2 M phosphate buffer, pH 7.0, applied potential −0.3 V

H_2O_2 produces distinct current response. On the contrary, no obvious current response can be observed for AA, DA, UA (Fig. 5a), QC, TP and Ca^{2+} (Fig. 5b). The results highlight a superior selectivity of the biosensor toward H_2O_2. Moreover, the reproducibility and stability of the biosensor were investigated by monitoring current response to 0.1 μM H_2O_2 under the same experimental conditions (phosphate buffer, pH 7.0, scan rate: 0.1 $V{\cdot}s^{-1}$). As shown in Fig. S6A (in Supporting Information), five parallel prepared GCE/NH_2-CD-HRP/Nafions gave an RSD of 3.6% for the response to 0.1 μM H_2O_2 and the RSD was found to be 5.8% for 20 consecutive measurements using a same electrode. The modified electrode was tested after being stored at 4 °C for 24 days, in this case, about 84.9% of its initial current response remained (Fig. S6B in Supporting Information). The results suggested the good reproducibility and acceptable stability of the biosensor.

Real sample analysis

To evaluate the applicability of the biosensor for real sample assay, the concentrations of H_2O_2 in tap water and black tea (Kongshifu ice tea, www.masterkong.com.cn) were detected. Firstly, samples were diluted 10,000 times with phosphate buffer and deoxygenated for 30 min. Then, a certain amount of H_2O_2 was added into the solution and the H_2O_2 level was measured by GCE/NH_2-CD-HRP/Nafion. The recoveries, in the range of 97.6–106.7% can be found from Table S1, which confirm the feasibility of the biosensor for the determination of H_2O_2 in real samples.

Conclusions

In summary, a novel sensitive biosensor was developed based on the immobilization of HRP in NH_2-CDs matrix for the determination of H_2O_2. Amino-functionalized CDs can provide more active sites and a friendly microenvironment for HRP immobilization. Thus, the immobilized HRP remains its bioelectrocatalytic activity and such modified GCE exhibited direct electrochemical behavior towards the reduction of H_2O_2. The biosensor showed excellent analytical performances in the determination of H_2O_2 with the sensitivity of 145 $\mu A{\cdot}\mu M^{-1}{\cdot}cm^{-2}$ and low detection limit of 0.0018 μM. In addition, real sample analysis of H_2O_2 in tap water and black tea with good recovery attest the reliability of the method.

Acknowledgements This work is supported by the Priority Academic Program Development of Jiangsu Higher Education Institutions and the Project of Scientific and Technologic Infrastructure of Suzhou (SZS201207).

Compliance with ethical standards The author(s) declare that they have no competing interests.

References

1. Song HY, Ni YN, Kokot S (2013) A glassy carbon electrode modified with poly(anthranilic acid), poly(diphenylamine sulfonate) and CuO nano-particles for the sensitive determination of hydrogen peroxide. Microchim Acta 180:1263–1270. https://doi.org/10.1007/s00604-013-1053-0
2. Jia NQ, Lian Q, Wang ZY, Shen HB (2009) A hydrogen peroxide biosensor based on direct electrochemistry of hemoglobin incorporated in PEO–PPO–PEO triblock copolymer film. Sensors Actuators B Chem 137:230–234. https://doi.org/10.1016/j.snb.2008.10.011
3. Li M, Gao H, Wang X, Wang Y, Qi H, Zhang C (2017) A fluorinedoped tin oxide electrode modified with gold nanoparticles for electrochemiluminescent determination of hydrogen peroxide released by living cells. Microchim Acta 184:603–610. https://doi.org/10.1007/s00604-016-2051-9
4. Fusco G, Bollella P, Mazzei F, Favero G, Antiochia R, Tortolini C (2016) Catalase-baed modified graphite electrode for hydrogen peroxide detection in different beverages. J Anal Methods Chem 2016: 8174913. https://doi.org/10.1155/2016/8174913
5. Hasan F, Shah AA, Hameed A (2006) Industrial applications of microbial lipases. Enzym Microb Technol 39:235–251. https://doi.org/10.1016/j.enzmictec.2005.10.016
6. Castillo J, Gáspár S, Leth S, Niculescu M, Mortari A, Bontidean I, Soukharev V, Dorneanu SA, Ryabov AD, Csöregi E (2004) Biosensors for life quality: design, development and applications. Sensors Actuators B Chem 102: 179–194. https://doi.org/10.1016/j.snb.2004.04.084
7. Liu YD, Liu XH, Guo ZP, ZG H, Xue ZG, XQ L (2017) Horseradish peroxidase supported on porous graphene as a novel sensing platform for detection of hydrogen peroxide in living cells sensitively. Biosens Bioelectron 87:101–107. https://doi.org/10.1016/j.bios.2016.08.015
8. Thenmozhi K, Narayanan SS (2017) Horseradish peroxidase and toluidine blue covalently immobilized leak-free sol-gel composite biosensor for hydrogen peroxide. Mater Sci Eng C 70:223–230. https://doi.org/10.1016/j.msec.2016.08.075
9. Wu C, Liu Z, Sun HH, Wang X, Xu P (2016) Selective determination of phenols and aromatic amines based on horseradish peroxidase-nanoporous gold co-catalytic strategy. Biosens Bioelectron 79:843–849. https://doi.org/10.1016/j.bios.2016.01.026
10. Mao CJ, Chen XB, Niu HL, Song JM, Zhang SY, Cui RJ (2012) A novel enzymatic hydrogen peroxide biosensor based on Ag/C nanocables. Biosens Bioelectron 31:544–547. https://doi.org/10.1016/j.bios.2011.10.001
11. Zhao XJ, Mai ZB, Kang XH, Zou XY (2008) Direct electrochemistry and electrocatalysis of horseradish peroxidase based on clay-chitosan-gold nanoparticle nanocomposite. Biosens Bioelectron 23: 1032–1038. https://doi.org/10.1016/j.bios.2007.10.012
12. XY X, Ray R, YL G, Ploehn HJ, Gearheart L, Raker K, Scrivens WA (2004) Electrophoretic analysis and purification of fluorescent single-wall carbon nanotube fragments. J Am Chem Soc 126: 12736–12737. https://doi.org/10.1021/ja040082h
13. Pumera M, Sánchez S, Ichinose I, Tang J (2007) Electrochemical nanobiosensors. Sensors Actuators B Chem 123:1195–1205. https://doi.org/10.1016/j.snb.2006.11.016
14. Willner I, Baron R, Willner B (2007) Integrated nanoparticle-biomolecule systems for biosensing and bioelectronics. Biosens Bioelectron 22:1841–1852. https://doi.org/10.1016/j.bios.2006.09.018
15. Bollela P, Fusco G, Tortolini C, Sanzò G, Favero G, Gorton L, Antiochia R (2017) Beyond graphene:electrochemical sensors

and biosensors for biomarkers detection. Biosens Bioelectron 89:152–166. https://doi.org/10.1016/j.bios.2016.03.068
16. Mazzei F, Favero G, Bollella P, Tortolini C, Mannina L (2015) Recent trends in electrochemical nanobiosensors for environmental analysis. Int J Environ Health 7:267–291. https://doi.org/10.1504/IJENVH.2015.073210
17. Peng ZL, Han X, Li SH, Al-Youbi AO, Bashammakh AB, El-Shahawi MS, Leblanc RM (2017) Carbon dots: biomacromolecule interaction, bioimaging and nanomedicine. Coord Chem Rev 343: 256–277. https://doi.org/10.1016/j.ccr.2017.06.001
18. Lim SY, Shen W, Gao ZQCZ (2015) Carbo quantum dots and their applications. Chem Soc Rev 44:362–381. https://doi.org/10.1039/c4cs00269e
19. Cao L, Wang X, Meziani MJ, FS L, Wang HF, Luo PG, Lin Y, Harruff BA, Veca LM, Murray D, Xie SY, Sun YP (2007) Carbon dots for multiphoton bioimaging. J Am Chem Soc 129:11318–11319. https://doi.org/10.1021/ja0735271
20. Jin HL, Huang HH, He YH, Feng X, Wang S, Dai LM, Wang JC (2015) Graphene quantum dots supported by grapheme nanoribbons with ultrahigh electrocatalytic performance for oxygen reduction. J Am Chem Soc 137:7588–7591. https://doi.org/10.1021/jacs.5b03799
21. Ray SC, Saha A, Jana NR, Sarkar R (2009) J Phys Chem C 113: 18546–18551
22. Park Y, Yoo J, Lim B, Kwon W, Rhee SW (2016) Improving the functionality of carbon nanodots: doping and surface functionalization. J Mater Chem A 4:18546–18551. https://doi.org/10.1039/c6ta04813g
23. Sun XC, Lei Y (2017) Fluorescent carbon dots and their sensing applications. Trends Anal Chem 89:163–180. https://doi.org/10.1016/j.trac.2017.02.001
24. Ding CQ, Zhu AW, Tian Y (2014) Functional surface engineering of C-dots for fluorescent biosensing and in vivo bioimaging. Acc Chem Res 47:20–30. https://doi.org/10.1021/ar400023s
25. Baker SN, Baker GA (2010) Luminescent carbon nanodots: emergent nanolights. Angew Chem Int Ed 49:6726–6744. https://doi.org/10.1002/anie.200906623
26. Gowthaman NSK, Sinduja B, Karthikeyan R, Rubini K, John SA (2017) Fabrication of nitrogen-doped carbon dots for screening the purine metabolic disorder in human fluids. Biosens Bioelectron 94: 30–38. https://doi.org/10.1016/j.bios.2017.02.034
27. Wang YL, Wang ZC, Rui YP, Li MG (2015) Horseradish peroxidase immobilization on carbon nanodots/CoFe layered double hydroxides: direct electrochemistry and hydrogen peroxide sensing. Biosens Bioelectron 64:57–62. https://doi.org/10.1016/j.bios.2014.08.054
28. Li Y, Zhao Y, Cheng H, Hu Y, Shi G, Dai L, Qu L (2012) Nitrogen-doped graphene quantum dots with oxygen-rich functional groups. J Am Chem Soc 134:15–18. https://doi.org/10.1021/ja206030c
29. Yang YH, Cui JH, Zheng MT, CF H, Tan SZ, Xiao Y, Yang Q, Liu YL (2012) One-step synthesis of amino-functionalized fluorescent carbon nanoparticles by hydrothermal carbonization of chitosan. Chem Commun 48:380–382. https://doi.org/10.1039/c1cc15678k
30. Chowdhury D, Gogoi N, Majumdar G (2012) Fluorescent carbon dots obtained from chitosan gel. RSC Adv 2:12156–12159. https://doi.org/10.1039/c1ra21705h
31. Mao SX, Long YM, Li WF, YF T, Deng AP (2013) Core-shell structured Ag@C for direct electrochemistry and hydrogen peroxide biosensor applications. Biosens Bioelectron 48:258–262. https://doi.org/10.1016/j.bios.2013.04.026
32. Wang J, Wang CF, Chen S (2012) Amphiphilic egg-derived carbon dots: rapid plasma fabrication, pyrolysis process, and multicolor printing patterns. Angew Chem Int Ed 51:9297–9301. https://doi.org/10.1002/anie.201204381
33. Wang SF, Chen T, Zhang ZL, Shen XC, ZX L, Pang DW, Wong KY (2005) Direct electrochemistry and electrocatalysis of heme proteins entrapped in agarose hydrogel films in room-temperature ionic liquids. Langmuir 21:9260–9266. https://doi.org/10.1021/la050947k
34. Adams S, Higgins AM, Jones RAL (2002) Surface-mediated folding and misfolding of proteins at lipid/water interfaces. Langmuir 18:4854–4861. https://doi.org/10.1021/la0112413
35. Kang XH, Wang J, Wu H, Aksay IA, Liu J, Lin YH (2009) Glucose oxidase-graphene-chitosan modified electrode for direct electrochemistry and glucose sensing. Biosens Bioelectron 25:901–905. https://doi.org/10.1016/j.bios.2009.09.004
36. Ren XL, Meng XW, Chen D, Tang FQ, Jiao J (2005) Using silver nanoparticle to enhance current response of biosensor. Biosens Bioelectron 21:433–437. https://doi.org/10.1016/j.bios.2004.08.052
37. Ko S, Takahashi Y, Fujita H, Tatsuma T, Sakoda A, Komori K (2012) Peroxidase-modified cupstacked carbon nanofiber networks for electrochemical biosensing with adjustable dynamic range. RSC Adv 2:1444–1449. https://doi.org/10.1039/c1ra00649e
38. Harbury HA (1957) Oxidation-reduction potentials of horseradish peroxidase. J Biol Chem 225:1009–1024
39. Dai HX, Lv WJ, Zuo XW, Zhu Q, Pan CJ, Niu XY, Liu JJ, Chen HL, Chen XG (2017) A novel biosensor based on boronic acid functionalized metal-orgnic frameworks for the determination of hydrogen peroxide released from living cells. Biosens Bioelectron 95:131–137. https://doi.org/10.1016/j.bios.2017.04.021
40. Ren QQ, Wu J, Zhang WC, Wang C, Qin X, Liu GC, Li ZX, Yu Y (2017) Real-time in vitro detection of cellular H_2O_2 under camptothecin stress using horseradish peroxidase, ionic liquid, and carbon nanotube-modified carbon fiber ultramicroelectrode. Sensors Actuators B Chem 245:615–621. https://doi.org/10.1016/j.snb.2017.02.001
41. Liu H, Guo K, Duan CY, Chen XJ, Zhu ZF (2016) A novel biosensor based on the direct electrochemistry of horseradish peroxidase immobilized in the three dimensional flower-like Bi_2WO_6 microspheres. Sci Eng C 64: 243–248. https://doi.org/10.1016/j.msec.2016.03.079
42. CM Y, Wang L, Li WB, Zhu C, Bao N, HY G (2015) Detection of cellular H_2O_2 in living cells based on horseradish peroxidase at the interface of Au nanoparticles decorated grapheme oxide. Sensors Actuators B Chem 211:17–24. https://doi.org/10.1016/j.snb.2015.01.064
43. Song HY, Ni YN, Kokot S (2014) Investigations of an electrochemical platform based on the layered MoS_2-graphene and horseradish peroxidase nanocomposite for direct electrochemistry and electrocatalysis. Biosens Bioelectron 56:137–143. https://doi.org/10.1016/j.bios.2014.01.014
44. Kaçar C, Dalkiran B, Erden PE, Kiliç E (2014) An amperometric hydrogen peroxide biosensor based on Co_3O_4 nanoparticles and multiwalled carbon nanotube modified glassy carbon electrode. Appl Surf Sci 311:139–146. https://doi.org/10.1016/j.apsusc.2014.05.028